JVI Journals.ASM.org

Simultaneous Treatment of Human Bronchial Epithelial Cells with Serine and Cysteine Protease Inhibitors Prevents Severe Acute Respiratory Syndrome Coronavirus Entry

Miyuki Kawase,[a] Kazuya Shirato,[a] Lia van der Hoek,[c] Fumihiro Taguchi,[b] and Shutoku Matsuyama[a]

Department of Virology III, National Institute of Infectious Diseases, Murayama Branch, Gakuen Musashi-Murayama, Tokyo, Japan[a]; Faculty of Veterinary Medicine, Nippon Veterinary and Life Science University, Kyonan-cho, Musashino, Tokyo, Japan[b]; and Department of Medical Microbiology, University of Amsterdam, Faculty of Earth and Life Sciences, Amsterdam, The Netherlands[c]

The type II transmembrane protease TMPRSS2 activates the spike (S) protein of severe acute respiratory syndrome coronavirus (SARS-CoV) on the cell surface following receptor binding during viral entry into cells. In the absence of TMPRSS2, SARS-CoV achieves cell entry via an endosomal pathway in which cathepsin L may play an important role, i.e., the activation of spike protein fusogenicity. This study shows that a commercial serine protease inhibitor (camostat) partially blocked infection by SARS-CoV and human coronavirus NL63 (HCoV-NL63) in HeLa cells expressing the receptor angiotensin-converting enzyme 2 (ACE2) and TMPRSS2. Simultaneous treatment of the cells with camostat and EST [(23,25)*trans*-epoxysuccinyl-L-leucylamindo-3-methylbutane ethyl ester], a cathepsin inhibitor, efficiently prevented both cell entry and the multistep growth of SARS-CoV in human Calu-3 airway epithelial cells. This efficient inhibition could be attributed to the dual blockade of entry from the cell surface and through the endosomal pathway. These observations suggest camostat as a candidate antiviral drug to prevent or depress TMPRSS2-dependent infection by SARS-CoV.

Both the severe acute respiratory syndrome coronavirus (SARS-CoV) and human coronavirus NL63 (HCoV-NL63) utilize angiotensin-converting enzyme 2 (ACE2) as an essential receptor for cell entry. Although ACE2 is present in the vesicular endothelial cells of all organs, these viruses are highly pathogenic only in the lungs. Furthermore, for SARS-CoV, the distribution of ACE2 does not strictly correlate with viral cell tropism. While ACE2 expression in the lungs has been shown in both type I and type II pneumocytes, the cell tropism of SARS-CoV has only been shown in type I pneumocytes during the early stages of infection (13, 19, 32). Therefore, it is predicted that both the receptor and a cofactor are required for viral entry into pneumocytes. Host cellular proteases play a critical role in the process of SARS-CoV entry into cells. Specifically, cathepsin L, trypsin, elastase, TMPRSS11a, hypoxanthine-aminopterin-thymidine (HAT), and TMPRSS2 activate the SARS-CoV spike (S) protein, which is a prerequisite for the fusion of viral and host cell membranes during viral entry (1, 2, 6, 15–17, 19, 20, 23, 27–30).

TMPRSS2 is expressed on the epithelial cells of human lungs (15, 19, 24), and its ability to activate viral glycoproteins has also been reported for influenza A virus, metapneumovirus, and porcine epidemic diarrhea virus (PEDV) (3–5, 7–12, 25, 26). The difference between these viruses and SARS-CoV occurs during the virus replication stage, during which viral glycoproteins are cleaved by proteases. The protease makes a simple cut in the glycoprotein during the maturation of the influenza A virus and metapneumovirus, in a manner similar to that made by furin. In the case of PEDV, TMPRSS2 enhances the release of viral particles into the culture fluid (25). In contrast, SARS-CoV spike (S) protein is predicted to be cleaved by TMPRSS2 following receptor binding for virus cell entry, which expected from the study for the S protein activation by trypsin (29). Recently, Bertram reported that HAT activates SARS-CoV S protein both in *cis* and in *trans* for cell-cell fusion, whereas TMPRSS2 activates S protein for cell-cell and virus-cell fusion in *trans* only (4). The multiple protease cleavage sites within the SARS-S protein are reportedly located closer to the C-terminal region than the putative cleavage sites of other coronaviruses (1, 4, 19, 27, 33); however, the site cleaved by TMPRSS2 for S protein activation has yet to be precisely identified.

Protease availability appears to determine the route of cell entry of SARS-CoV. In the absence of proteases at the cell surface, SARS-CoV enters cells by an endosomal pathway and the S protein is fusogenically activated by cathepsin L, thereby allowing fusion of the viral and endosome membranes (17, 19, 30). In contrast, in the presence of proteases such as trypsin, elastase, and TMPRSS2, which induce envelope-plasma membrane fusion, SARS-CoV enters the cell cytoplasm directly from the cell surface (19, 27). Despite these observations, the precise mechanisms by which SARS-CoV penetrates the cell surface are currently unknown; however, it is possible that entry is via an early endosome, similar to that reported for HIV (22). Based on the importance of TMPRSS2 for S protein activation, the aim of the present study was to identify an inhibitor of TMPRSS2 from commercial drugs that could prevent SARS-CoV and HCoV-NL63 infection in cell culture as well as in humans.

MATERIALS AND METHODS

Cells and viruses. HeLa cells expressing both ACE2 and TMPRSS2 (HeLa-ACE2-TMPRSS2) were prepared by cotransfecting HeLa229 cells

Received 17 January 2012 **Accepted** 30 March 2012
Published ahead of print 11 April 2012
Address correspondence to Shutoku Matsuyama, matuyama@nih.go.jp.

doi:10.1128/JVI.00094-12

with a pTargeT plasmid (Promega, Madison, WI) harboring the human ACE2 gene and a pcDNA plasmid harboring the human TMPRSS2 gene, followed by selection in a medium containing G418. HeLa229 cells expressing only ACE2 (HeLa-ACE2) were established by transfecting the cells with a plasmid carrying the ACE2 gene. The cells were grown and maintained in Dulbecco's modified Eagle's medium (DMEM; Nissui, Tokyo, Japan) supplemented with 5% fetal bovine serum (Sigma, St. Louis, MO). Human bronchial epithelial Calu-3 cells were grown in modified Eagle's medium (MEM) supplemented with 10% fetal calf serum (FCS) as recommended by the American Tissue Culture Collection (ATCC). The SARS-CoV Frankfurt 1 strain was propagated and assayed using Vero E6 cells, as previously described (20). The HCoV-NL63 strain was propagated and assayed using LLC-MK2 cells as previously described (16). Pseudotyped vesicular stomatitis virus (VSV) expressing green fluorescent protein (GFP) and harboring SARS-CoV S protein or VSV-G protein was prepared as previously described (14). The production of a VSV pseudotype bearing the NL63-S protein is described below.

Generation of VSV pseudotyped with NL63-S protein. The S protein of SARS-CoV with a C-terminal 19-amino-acid deletion has been reported to efficiently incorporate into VSV-based pseudotyped virus (14). Therefore, we tried to generate VSV-based pseudotyped virus bearing NL63-S protein using this C-terminally truncated S protein. The cDNA fragment of the full-size S protein, or the S protein with a ≥19-amino-acid truncation from the C terminus, was amplified by reverse transcription-PCR (RT-PCR) and cloned into the mammalian expression vector pTargeT. In addition, the TransIT-293 transfection reagent (Mirus Bio, Madison, WI) was used to transfect 293T/17 cells, obtained from the ATCC (CRL-11268) with the expression plasmid, followed by incubation at 37°C for 30 to 36 h. These cells were then infected with VSV[Delta]G-G, which encodes the VSV-G protein, but with replacement of the gene by a GFP gene (kindly provided by M. A. Whitt, GTx, Inc., Memphis, TN) and were incubated at 37°C for 1 h. After four washes with phosphate-buffered saline (PBS), the cells were further incubated at 37°C for 24 h. The culture fluid was collected, centrifuged at 1,000 rpm for 5 min at 4°C, aliquoted into cryotubes, and stored at −80°C until use. The controls were VSV-pseudotyped viruses bearing VSV-G proteins, generated as previously reported (14). The infectivity of the pseudotyped viruses was determined by counting the number of GFP-positive cells and expressed as infectious units (IU). Finally, we chose the pseudotyped NL63-S (with a 24-amino-acid truncation) as it efficiently infected HeLa-ACE2, but not HeLa, cells.

Inhibitors. The following inhibitors were used in this study: benzamidine hydrochloride (A1380; AppliChem), aprotinin (A213; AppliChem), tosyl lysyl chloromethyl ketone (TLCK) (BML-Pl121; Enzo Life Sciences), gabexate mesylate (G2417; Sigma), EST [(23,25)*trans*-epoxysuccinyl-L-leucylamindo-3-methylbutane ethyl ester] (330005; Calbiochem), bafilomycin A1 (B1793; Sigma), MDL28170 (M6690; Sigma), cathepsin L inhibitor III (219427; Calbiochem), leupeptin (11017101001; Roche), cytochalasin D (C8273; Sigma), and camostat mesylate (3193; Tocris Bioscience). The concentrations are specified in the figure legends.

Pseudotyped virus entry assay. HeLa-ACE2 or HeLa-ACE2-TMPRSS2 cells in 96-well plates were treated with growth medium containing the above-described inhibitors for 30 min at 37°C. Approximately 10^3 IU of virus was then used to infect 10^5 cells in the presence of the inhibitors. The cells were then cultured at 37°C for 20 h. GFP-positive cells were photographed under a fluorescence microscope (Keyence Corporation, Osaka, Japan) and counted using image measurement and analysis software (VH-H1A5 version 2.6; Keyence). The inhibitory effect was calculated by counting the number of GFP-positive cells, as previously described (18).

Quantification of transcripts. The mRNAs for ACE2, HAT, and TMPRSS2 were compared in Calu-3 cells and human lung cells. Human lung cell total RNA, isolated from three male and three female Caucasians ages 32 to 61 years, was purchased from Clontech (636524). In addition, cellular Calu-3 RNA was isolated using the Isogen reagent (Nippon Gene) according to the manufacturer's protocol. The TMPRSS2 mRNA fragment was amplified with the oligonucleotide pair 5′-CTCTACGGACCAAACTTCATC-3′ and 5′-CCACTATTCCTTGGCTAGAGTAA-3′, and hybridization was detected with the probes 5′-TCAGAGGAAGTCCTGGCACCCTGTGTG-3′ (3′-fluorescein isothiocyanate [FITC] labeled) and 5′-CAAGACGACTGGAACGAGAACTACGGGC-3′ (5′-LCRed640 labeled). The HAT mRNA fragment was amplified using the oligonucleotide pair 5′-CTTGTGAGACTTGAGAACAGTG-3′ and 5′-ACCTGTCCTTGCCTTAGC-3′, and hybridization was detected with the probes 5′-GCCAGCATATTCTTGAGCGCCCCA-3′ (3′-FITC labeled) and 5′-CCTGTTACATAAGCAGTAGAGCCAGGTGGAAT-3′ (5′-LCRed640 labeled). The amount of ACE2 mRNA was estimated using the oligonucleotide pair 5′-CCGTATCAATGATGCTTTCCG-3′ and 5′-CAGTGAAGATCAGGATGACAATG-3′, and hybridization was detected with the probes 5′-ACCTCCTAACCAGCCCCCTGTTTCCATA-3′ (3′-FITC labeled) and 5′-GGCTGATTGTTTTTGGAGTTGTGATGGGAG-3′ (5′-LCRed640 labeled). PCR analysis was performed in a LightCycler instrument (Roche Diagnostics). The mRNA copy number was calculated based on a calibration line obtained by 10-fold stepwise dilution of plasmid DNA.

Knockdown of TMPRSS2 and HAT. Calu-3 cells with knocked-down human TMPRSS2, HAT, or a nontargeting control were generated using the respective small interfering RNA (siRNA) oligonucleotides (E-006048-00, E-005894-00, and D-001910-10-05; Dharmacon) in a transient transfection carried out according to the manufacturer's protocol. Knockdown of human TMPRSS2 or HAT was estimated by real-time PCR.

Authentic SARS-CoV entry assay. HeLa-ACE2, HeLa-ACE2-TMPRSS2, and Calu-3 cells in 96-well plates were treated with DMEM containing inhibitors at 37°C for 30 min. Approximately 10^3 PFU of SARS-CoV (see Fig. 2B), 10^1 PFU of HCoV-NL63 (Fig. 2B), and 10^6 PFU of SARS-CoV (see Fig. 9 and 10) in DMEM plus inhibitors were used to infect 10^5 cells, which were then cultured at 37°C for 5 h. Cellular RNA was isolated by the addition of 200 μl of Isogen reagent (Nippon Gene). Real-time PCR was performed to estimate the amount of newly synthesized mRNA9 of SARS-CoV, as previously described (19). The mRNA9 for SARS-CoV was amplified using the oligonucleotide pair 5′-CTCGATCTCTTGTAGATCTG-3′ and 5′-TCTAAGTTCCTCCTTGCCAT-3′, and hybridization was detected with the probes 5′-ACCAGAATGGAGGACGCAATGGGGCAAG-3′ (3′-FITC labeled) and 5′-CCAAAACAGCGCCGACCCCAAGGTTTAC-3′ (5′-LCRed640 labeled). The mRNA9 of HCoV-NL63 was amplified using the oligonucleotide pair 5′-TTAGACTTTGTGTCTACTC-3′ and 5′-TACGCCAACGCTCTTGAAC-3′, and hybridization was detected with the probes 5′-TTATTACCCTTACCAATAGGGACAAGATTCCTGGG-3′ (3′-FITC labeled) and 5′-ATGACCCTATATGGTGCCTTATCAGAACTAACCAAAAG-3′ (5′-LCRed640 labeled). PCR analysis was performed in a LightCycler instrument (Roche Diagnostics). Viral mRNA levels were normalized to the expression levels of the cellular housekeeping gene coding for glyceraldehyde-3-phosphate dehydrogenase (GAPDH).

Multistep growth of authentic SARS-CoV. Subconfluent Calu-3 cells (10^6 cells) were inoculated into 24-well plates with 10^4 PFU of SARS-CoV in DMEM and incubated for 2 h at 37°C. Residual virus was then removed, and the medium was replaced with fresh medium with 10 μM cathepsin inhibitor EST, 10 μM camostat, or both. Cellular RNA was isolated from the cells from four wells every 24 h for 6 days by adding 400 μl of Isogen reagent. The growth kinetics of SARS-CoV were estimated by measuring viral mRNA9 using real-time PCR as previously described (20).

RESULTS

Cell entry of pseudotyped viruses in the presence of exogenous trypsin or TMPRSS2. A nonenzymatic cell dissociation solution (C5914; Sigma), rather than trypsin, was used for passaging cells, as exogenous trypsin may lead to an overestimation of the level of human coronavirus infection. Protease-dependent cell entry of coronaviruses into HeLa cells stably expressing human ACE2 was estimated as follows. First, VSV pseudotypes bearing SARS-S, NL63-S, or VSV-G were treated with trypsin (TLCK treated) (T-8802; Sigma) for 5 min at 37°C and then inoculated into the cells

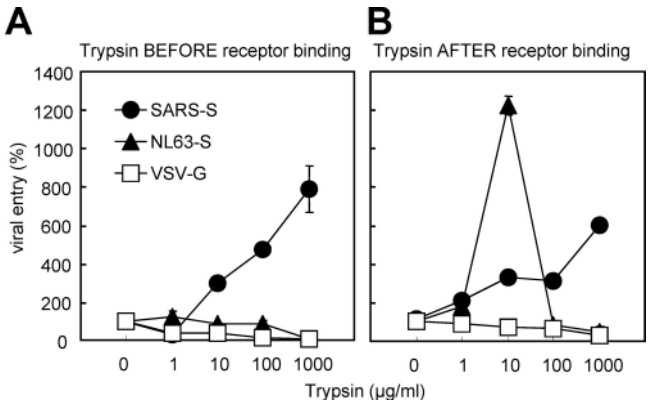

FIG 1 Enhancement of protease-mediated viral entry into cells. (A) Pseudotyped viruses bearing SARS-S, NL63-S, or VSV-G were incubated with serially diluted trypsin for 5 min at 37°C, followed by inoculation onto HeLa-ACE2 cells for 30 min on ice. (B) Pseudotyped viruses were first adsorbed onto HeLa-ACE2 cells for 30 min on ice, followed by the addition of serial dilutions of trypsin to cells and incubation for a further 5 min at 37°C. The medium was then changed, and the cells were incubated for 20 h at 37°C. Infectivity was quantified by counting GFP-positive cells. The results are presented as the percentage of infected cells (at least 50 GFP-positive cells were counted). Error bars indicate the standard deviations (SD) of the means from four independent wells.

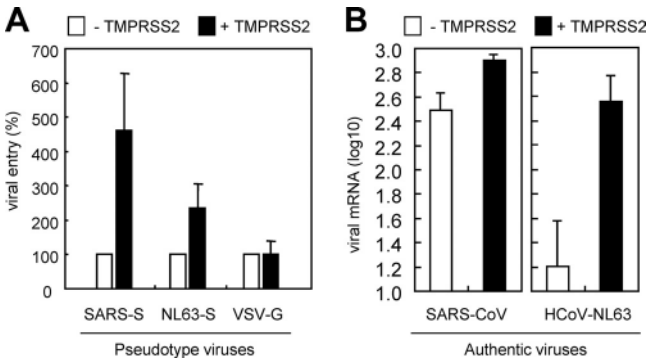

FIG 2 Effect of TMPRSS2 on virus entry into cells. (A) Pseudotyped viruses were inoculated onto HeLa-ACE2 (white bars) and HeLa-ACE2-TMPRSS2 (black bars) cells. Infectivity was quantified by counting GFP-positive cells 20 h after viral inoculation. The results are presented as the percentage of infected HeLa-ACE2 cells (at least 50 GFP-positive cells were counted). Error bars indicate the SD of the means from eight independent samples. (B). Authentic SARS-CoV and HCoV-NL63 were inoculated onto HeLa-ACE2 (white bars) and HeLa-ACE2-TMPRSS2 (black bars) cells. Infectivity was quantified by real-time PCR to measure the viral mRNA9 of these viruses. Error bars indicate the SD of the means from four independent samples.

for 30 min on ice. The medium was then changed, and the cells were incubated for 20 h at 37°C. Infection by pseudotyped virus was monitored by GFP expression. Figure 1A shows that whereas a high concentration of trypsin (1 mg/ml) inactivated pseudotyped virus bearing NL63-S, it activated SARS-S-bearing virus. Thus, unlike NL63-S, SARS-S is resistant to trypsin and may be activated by cleavage after receptor binding. Second, pseudotyped viruses were adsorbed onto cells for 30 min on ice, followed by the addition of trypsin for 5 min at 37°C. Pseudotyped SARS-S on the cell surface was activated by trypsin in a concentration-dependent manner, whereas strong activation of NL63-S occurred only at a concentration of 10 μg/ml (Fig. 1B). Third, we evaluated whether cell entry by the viruses was enhanced by TMPRSS2. HeLa-ACE2 or HeLa-ACE2-TMPRSS2 cells were infected with pseudotyped viruses. Figure 2A shows the averages derived from the control data in this study, i.e., pseudotyped virus infection in the absence of inhibitors. Pseudotyped SARS-S entry increased 5-fold in the presence of TMPRSS2, and pseudotyped NL63-S entry increased by 2.5-fold. VSV infection was not affected by TMPRSS2. To facilitate comparison of the decrease in infection due to inhibitors between the experiments, these control data (pseudotyped virus entry into HeLa-ACE2 and HeLa-ACE2-TMPRSS2 cells in the absence of inhibitors) were assumed to represent 100% viral entry in the following figures. Furthermore, cell entry by authentic SARS-CoV and HCoV-NL63 was also tested, and real-time PCR was used to detect the newly synthesized viral mRNA9. Figure 2B shows that SARS-CoV entry increased 2.6-fold and HCoV-NL63 entry increased 23-fold in the presence of TMPRSS2.

Effects of serine protease inhibitors on viral entry. The specific inhibitory effects of chemicals on TMPRSS2 were examined by observing their ability to suppress cell entry by pseudotyped virus. HeLa-ACE2 or HeLa-ACE2-TMPRSS2 cells were treated with benzamidine, aprotinin, gabexate, camostat, and TLCK for 30 min and then inoculated with pseudotyped viruses in the continued presence of these inhibitors. Figure 3A shows that only camostat blocked the entry of pseudotyped SARS-S and NL63-S into TMPRSS2-expressing cells. Suppression by TLCK was not restricted to TMPRSS2-expressing cells since TLCK inhibited pseudotyped SARS-S and NL63-S in both HeLa-ACE2 and HeLa-ACE2-TMPRSS2 cells, indicating that TLCK targets not only TMPRSS2 but cathepsins as well. The concentration-dependent effect of camostat on viral entry was compared with that of its analog, gabexate, in Fig. 3B. Camostat-mediated suppression of SARS-S entry never exceeded 65%, even in the presence of a high concentration of the drug (100 μM), indicating that, despite the presence of TMPRSS2, 35% of the viruses utilized endosomal cathepsins for cell entry. In contrast, in the absence of TMPRSS2, camostat had insignificant effects on pseudotyped virus entry. Similar results were seen for NL63-S.

To confirm the effects of camostat on S protein activation, we examined the inhibition of syncytium formation. Plasmids pKS/SARS-S and pTarget/NL63-S were transfected into HeLa-ACE2-TMPRSS2 cells with pEGFP plasmids to visualize transfected cells. These cells were then cultured in the presence of serially diluted camostat. After 22 h, syncytia were observed in SARS-S- and NL63-S-transfected cells, but their formation was inhibited by camostat (Fig. 4A). Nuclei were stained with 4′,6-diamidino-2-phenylindole (DAPI), and the extent of syncytium formation was quantified by counting the number of nuclei in the fused cells (eight syncytia). Syncytium formation was moderately inhibited by camostat at concentrations of 0.1 μM and 1 μM and completely inhibited at a concentration of 10 μM (Fig. 4B). These results indicated that camostat prevents the activation of S protein at the cell surface.

Effects of cathepsin inhibitors on viral entry. SARS-CoV utilizes endosomal cathepsin L, and infection is blocked by cathepsin L inhibitors (30). In contrast, HCoV-NL63 does not utilize endosomal cathepsin L (16). EST, a broad inhibitor of cysteine proteases, including cathepsins, is also unable to block infection by NL63 (16). Here, we examined the inhibition of viral entry in the presence of EST, MDL, cathepsin L inhibitor III (LIII), and leupeptin (Leu). Two other inhibitors, bafilomycin A1, which blocks

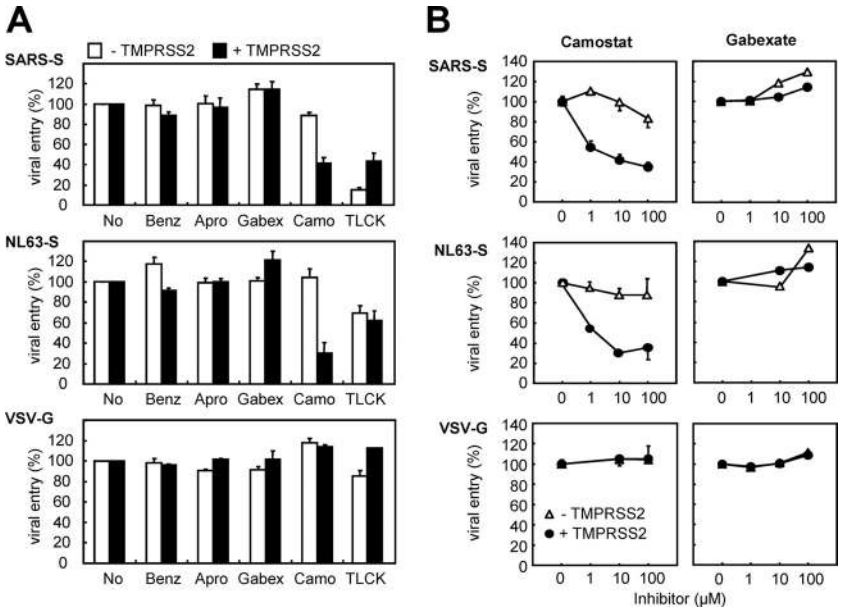

FIG 3 Effects of serine protease inhibitors on viral entry and syncytium formation. (A) HeLa-ACE2 (white bars) and HeLa-ACE2-TMPRSS2 (black bars) cells were infected with pseudotype viruses bearing SARS-S, NL63-S, or VSV-G in the presence of 10 μM benzamidine (Benz), 10 μM aprotinin (Apro), 10 μM gabexate (Gabex), 10 μM camostat (Camo), or 50 μM TLCK. (B) Concentration-dependent effects of inhibitors in HeLa-ACE2 (triangles) or HeLa-ACE2-TMPRSS2 (circles) cells infected with pseudotyped viruses bearing SARS-S, NL63-S, or VSV-G in the presence of serially diluted camostat or gabexate. Infectivity was quantified by counting GFP-positive cells 20 h after viral inoculation. The results are presented as a percentage of infection (at least 200 GFP-positive cells were counted for untreated [No] cells), and error bars indicate the SD of the means from four independent wells.

the acidification of endosomes and thereby also cathepsins, and cytochalasin D, which prevents actin polymerization and therefore endosomal trafficking, were also tested. Figure 5A shows that infection of TMPRSS2-negative cells (white bars) by pseudotyped SARS-S was inhibited about 80% by LIII, but infection by pseudotyped NL63 was only inhibited by 15%. These rates of inhibition are similar to those reported previously (16). Interestingly, inhibition of NL63-S cell entry by bafilomycin A1, EST, and MDL was similar to that of SARS-S cell entry by the same compounds; these results are different from previously reported results (16). Therefore, we carefully tested the concentration-dependent effects of EST and LIII to confirm this difference. Suppression of NL63-S entry was about 80% in the presence of 10 μM to 100 μM EST, but no significant suppression by LIII was observed (Fig. 5B). These results indicate that NL63 utilizes a cysteine protease other than cathepsin L for cell entry.

On the other hand, infection of TMPRSS2-expressing cells (black bars) with pseudotyped SARS-S was inhibited by 30 to 40% in the presence of cathepsin inhibitors and bafilomycin A1, whereas this was not observed for NL63-S infection, except in the

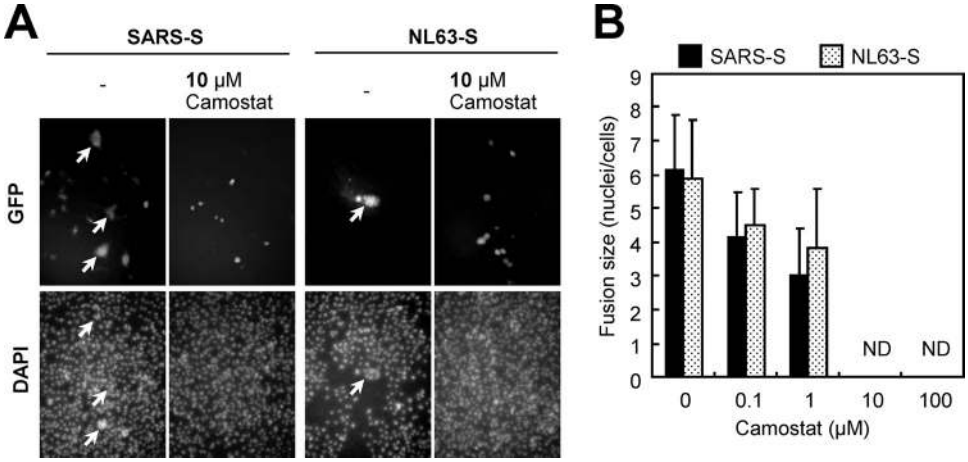

FIG 4 Inhibition of syncytium formation by camostat. (A) Plasmids encoding SARS-S or NL63-S were transfected with plasmid encoding enhanced green fluorescent protein (EGFP) in HeLa-ACE2-TMPRSS2 cells, and incubated in the presence or absence of 10 μM camostat. After 20 h, the cells were fixed with 4% formalin and stained with DAPI. (B) The sizes of syncytia in the absence or presence of 0.1, 1, 10, or 100 μM camostat were quantified by counting the number of nuclei in the fused cells. Error bars indicate the SD of the means from 10 independent syncytia. ND, not determined.

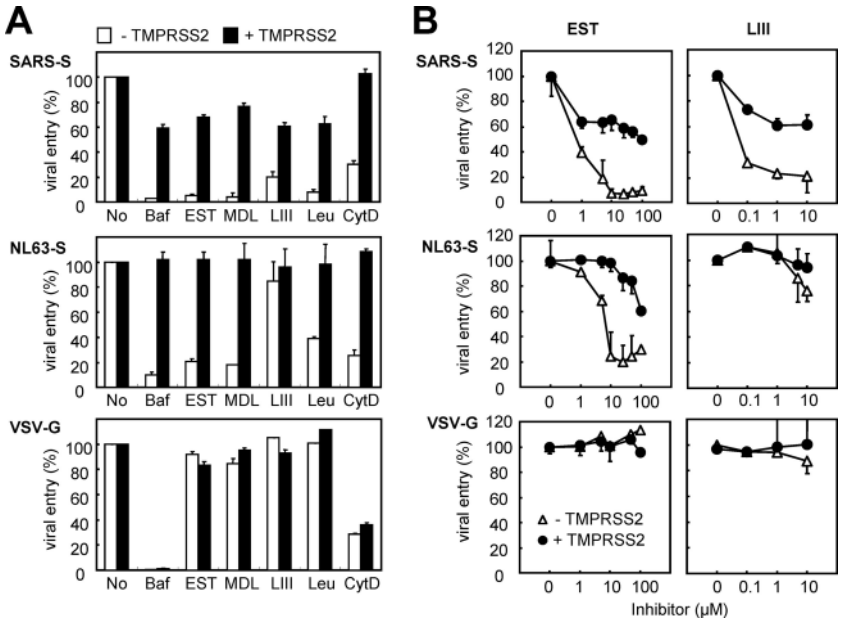

FIG 5 Effects of cathepsin inhibitors or endosome-tropic inhibitors on viral entry. HeLa-ACE2 (white bars) and HeLa-ACE2-TMPRSS2 (black bars) cells were infected with pseudotyped viruses bearing SARS-S, NL63-S, or VSV-G in the presence of 100 nM bafilomycin A1 (Baf), 10 μM EST, 50 μM MDL28170 (MDL), 5 μM cathepsin L inhibitor III (LIII), 50 μM leupeptin (Leu), or 1 μM cytochalasin D (CytD). Infectivity was quantified by counting GFP-positive cells 20 h after viral inoculation. The results are presented as a percentage of infection (at least 200 GFP-positive cells were counted for untreated [No] cells), and error bars indicate the SD of the means from four independent wells.

case of cathepsin L inhibitor III, which inhibited infection by about 15%. These results indicate that 60 to 70% of SARS-S viruses utilize TMPRSS2 rather than cathepsins, whereas 100% of NL63-S viruses utilize TMPRSS2 rather than cathepsins. Furthermore, pseudotyped viruses bearing SARS-S and NL63-S were not inhibited by cytochalasin D in TMPRSS2-expressing cells, although viral inhibition was reduced by >70% in TMPRSS2-negative cells. These results indicated that, in the presence of TMPRSS2, pseudotyped viruses bearing SARS-S and NL63-S complete their entry between the cell surface and early endosome stages.

Inhibition of viral entry by simultaneous treatment with serine and cysteine protease inhibitors. The above results showed that inhibitors of serine and cysteine proteases partially blocked the infection of pseudotyped viruses bearing SARS-S and NL63-S into TMPRSS2-expressing cells. It was therefore of interest to evaluate the effects of simultaneous treatment with both inhibitors on viral entry. TMPRSS2-expressing cells were incubated in medium containing 10 μM EST, 10 μM camostat, or both for 30 min and then infected with the pseudotyped viruses in the presence of inhibitors. Figure 6 shows that simultaneous treatment with camostat and EST dramatically blocked infection, with a decrease of >95%. Similar results were obtained using bafilomycin A1 instead of EST.

Next, we examined the entry speed of these pseudotyped viruses when treated with both EST and camostat. HeLa-ACE2 and HeLa-ACE2-TMPRSS2 were treated with the inhibitors to stop viral entry at the indicated time points after viral adsorption. Cell entry by pseudotyped SARS-S and NL63-S occurred 1 h earlier in cells expressing TMPRSS2 than in nonexpressing cells (Fig. 7). The entry speed of NL63 was slightly higher than that of SARS, as evidenced by the steeper curve for NL63 versus SARS.

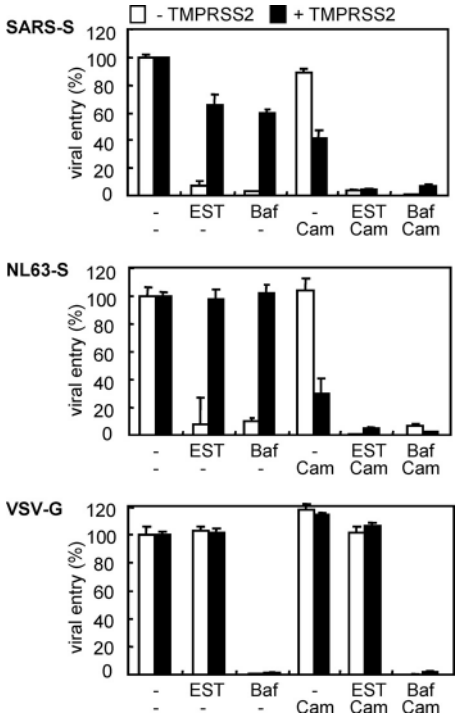

FIG 6 Inhibition of viral entry by simultaneous treatment with serine and cysteine protease inhibitors. HeLa-ACE2 (white bars) and HeLa-ACE2-TMPRSS2 (black bars) cells were infected with pseudotyped viruses bearing SARS-S, NL63-S, or VSV-G in the presence of 10 μM EST, 10 μM camostat (Cam), 100 nM bafilomycin (Baf), both EST and Cam, or both bafilomycin and camostat. Infectivity was quantified by counting GFP-positive cells 20 h after viral inoculation. The results are presented as a percentage of infection (at least 200 GFP-positive cells were counted for untreated cells), and error bars indicate the SD of the means from four independent wells.

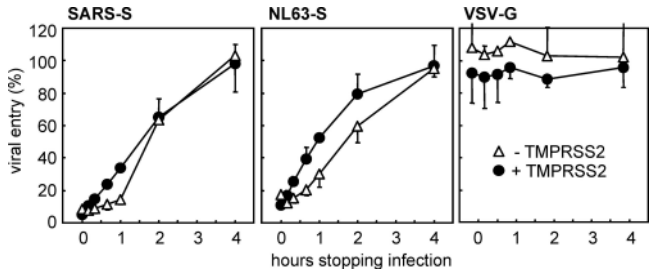

FIG 7 Cell entry kinetics of pseudotyped viruses. Pseudotyped viruses bearing SARS-S, NL63-S, or VSV-G were inoculated onto HeLa-ACE2 (triangles) and HeLa-ACE2-TMPRSS2 (circles) cells and treated with both 10 μM EST and 10 μM camostat to stop viral entry at the indicated time points. Infectivity was quantified by counting GFP-positive cells 20 h after viral inoculation. The results are presented as a percentage of infection (at least 500 GFP-positive cells were counted for untreated cells), and error bars indicate the SD of the means from four independent wells.

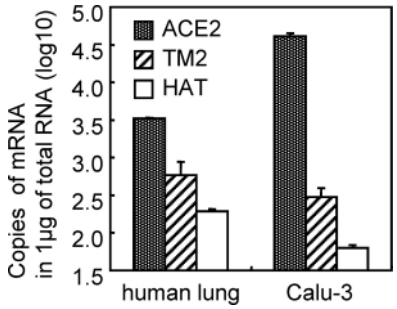

FIG 8 Comparison of transcripts in human lung and Calu-3 cells. The amounts of ACE2, TMPRSS2 (TM2), and HAT mRNA in human lungs or Calu-3 cells were measured using real-time PCR as described in Materials and Methods. Error bars indicate the SD of the means from six independent samples.

Cell entry and multistep growth of authentic SARS-CoV in Calu-3 cells. The above results were obtained in artificially constructed cells expressing TMPRSS2. Thus, the following experiments were performed in Calu-3 cells, an immortalized human airway epithelial cell line regularly used in the study of respiratory pathologies. Unfortunately, Calu-3 cells are not susceptible to VSV pseudotypes because the innate immunity of the cells is thought to suppress the early stages of viral infection. Similarly, Calu-3 is not susceptible to certain other human coronaviruses, such as OC43 and 229E (34), nor were we able to quantitatively determine the level of viral mRNA at 5 h after infection with authentic NL63 (data not shown). Interestingly, authentic SARS-CoV has been reported to infect Calu-3 cells because the SARS-CoV-encoded nsp1 protein suppresses the interferon regulatory factors (34). Therefore, authentic SARS-CoV and real-time PCR were used to detect viral entry and multistep viral growth.

First, ACE2, HAT, and TMPRSS2 mRNA levels were compared in Calu-3 cells and human lung cells. Figure 8 shows that ACE2 mRNA levels were significantly higher and those of TMPRSS2 mRNA were slightly lower in Calu-3 cells than in human lung cells, whereas HAT mRNA was barely detectable in the latter. To test whether SARS-CoV utilizes TMPRSS2 or HAT in Calu-3 cells, the siRNA technique was used to knock down these mRNAs. Calu-3 cells were transiently transfected with siRNAs, and the suppression of the target mRNAs was analyzed by real-time PCR (Fig. 9A). A nontargeting siRNA served as the negative control. However, nontargeting siRNA nonspecifically reduced ACE2, TMPRSS2, and HAT mRNA levels (Fig. 9A), thereby reducing SARS-CoV entry by 10-fold (Fig. 9B). Transfection with a TMPRSS2-specific siRNA resulted in a 10-fold specific decrease of TMPRSS2 mRNA and no effect on ACE2 mRNA in Calu-3 cells compared with nontargeting control transfections. The decrease in HAT mRNA obtained with a HAT-specific siRNA was not evaluated because the amount of remaining transcript was too low to be detectable (Fig. 9A).

Furthermore, SARS-CoV entry into Calu-3 cells was measured in cells treated with siRNA for 4 days followed by additional treatment with EST for 30 min. These cells were then inoculated with SARS-CoV at multiplicities of infection (MOI) of 10 (infectious units were estimated in Vero-E6 cells), and 5 h later, total cellular RNA was isolated. Viral entry was estimated based on newly synthesized viral mRNA9, which was measured quantitatively using real-time PCR. SARS-CoV entry into Calu-3 cells was 1,000-fold lower than that into Vero-E6 cells (data not shown), but was enough to be quantified by real-time PCR. Fig. 9C shows that TMPRSS2-specific siRNA caused efficient inhibition of SARS-CoV cell entry (5-fold decrease), whereas 10 μM EST caused no inhibition. Simultaneous treatment with siRNA and 10 μM EST blocked infection by 10-fold (Fig. 9C). Treatment of the cells with HAT-specific siRNA had no effect on SARS-CoV entry (Fig. 9C).

The effect on Calu-3 cells of simultaneous treatment with SARS-CoV entry inhibitors (i.e., camostat and EST) was also measured. Cells were treated with the inhibitors at 37°C for 30 min, inoculated with SARS-CoV at an MOI of 10, and incubated for 5 h in the presence of the inhibitors. Nontoxic concentrations of inhibitors were used for the experiments in Fig. 10A and C; this was confirmed by measuring mRNA levels of ACE2 and GAPDH by real-time PCR (Fig. 10B and D). Figure 10A shows that 10 μM camostat caused efficient inhibition of viral entry, with a 10-fold decrease, whereas no significant inhibition of SARS-CoV cell entry was obtained with 10 μM EST. However, simultaneous treatment with camostat and EST dramatically blocked infection, with a decrease of 100-fold.

Finally, inhibition of the multistep growth of SARS-CoV was tested in Calu-3 cells. SARS-CoV (10^4 PFU) was inoculated onto 10^6 Calu-3 cells (MOI, 0.01) at 37°C for 2 h. The cells were washed twice with PBS and then incubated for 6 days in the presence or absence of inhibitors. Figure 10C shows that viral replication was suppressed >6,000-fold in cells cultured in the presence of both 10 μM camostat and 10 μM EST. When provided alone, camostat caused a 13-fold decrease in SARS-CoV replication, while EST alone caused a 33-fold decrease. These results indicated that simultaneous treatment with serine and cysteine protease inhibitors efficiently blocked SARS-CoV infection in a human airway epithelial cell line.

DISCUSSION

The interaction of SARS-CoV with host proteases is receptor mediated since the protease cleavage site of S protein is thought to be exposed only after receptor binding (17, 19, 30). During the initial stage of infection, viral utilization of the TMPRSS2 allows for tight temporal control over fusion by protecting the activating cleavage site from premature proteolysis while still allowing efficient cleavage once the virus has bound to target cell receptors. Interestingly, Shulla et al. reported that TMPRSS2 is closely linked to the viral

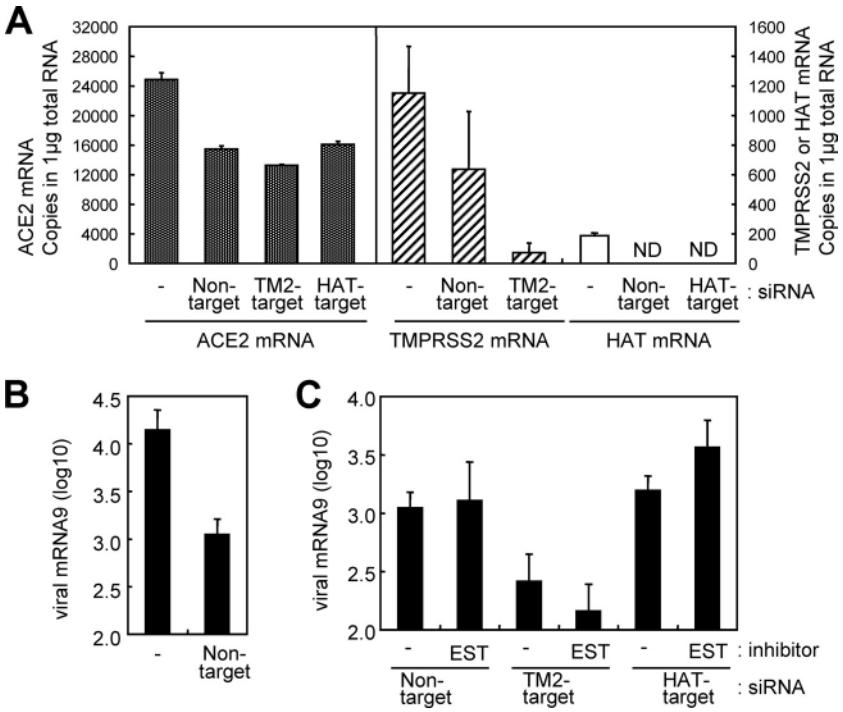

FIG 9 Effect of TMPRSS2 and HAT siRNA-mediated knockdown on SARS-CoV entry into Calu-3 cells. (A) The cells were transiently transfected with siRNAs targeting TMPRSS2 (TM2-target) or HAT (HAT-target) or a nontargeting control ("Non-target"). Nontransfected cells served as the negative control (−). Four days after transfection, cellular RNA was isolated, and ACE2, TMPRSS2, and HAT mRNAs were measured by real-time PCR. (B) Calu-3 cells were infected with SARS-CoV 4 days after transfection of a nontargeting siRNA or nontransfected control (−). Cellular RNA was isolated 5 h after infection, and infectivity was quantified by real-time PCR. (C) Four days after the above-described transfection with siRNA, Calu-3 cells were infected with SARS-CoV in the presence or absence of 10 μM EST. Cellular RNA was isolated 5 h after infection, and infectivity was quantified by real-time PCR measurement of the amount of viral mRNA9. Error bars indicate the SD of the means from six independent samples.

receptor on the target cell surface (27). In the present study, the protease sensitivity of NL63 differed from that of SARS-CoV (Fig. 1). Pseudotyped viruses bearing NL63-S were inactivated by pretreatment with trypsin before cell adsorption, whereas after adsorption, activation occurred only in the presence of a specific concentration of the protease. In contrast, a high concentration of trypsin (1 mg/ml) activated SARS-S infection, indicating that the SARS-CoV S protein is resistant to trypsin (Fig. 1A and B). However, these results using SARS-S were contrary to the findings previously reported by Simmons et al., which showed that trypsin treatment reduced viral infectivity (28, 29). This may be because they added soybean trypsin inhibitor (STI) to stop proteolysis before virus inoculation, whereas we did not. Therefore, in our experiments, trypsin was still active after virus inoculation, indicating that SARS-S is resistant to very high concentrations of trypsin and it retains the ability of infection. Thus, during severe inflammation, NL63 may be inactivated by "free proteases," such as elastase, whereas SARS-CoV is activated. This would explain, at least in part, the different pathogenicities of these two viruses.

Our results indicate that the membrane-anchored protease TMPRSS2 enhances cell entry of both SARS-CoV and HCoV-NL63. NL63 appears to particularly favor TMPRSS2 rather than cathepsin, since in TMPRSS2-expressing cells, pseudotyped NL63-S entry was not inhibited by cathepsin inhibitors at concentrations sufficient to inhibit the infection of TMPRSS2-negative cells (Fig. 5A, middle panel, black versus white bars), although 30 to 40% of SARS-CoV was inhibited by the same inhibitors (Fig. 5A, top panel, black bars). Of note, the present finding of efficient inhibition of cell entry by pseudotyped NL63-S into EST-treated cells without TMPRSS2 (Fig. 5B, middle panel, white triangle) is contrary to previously reported data by Huang et al., (16). Also in contrast to previous results is our observation that bafilomycin A1 inhibited NL63-S entry, whereas ammonium chloride, which also blocks the acidification of endosomes and thereby also cathepsins, was reported not to cause inhibition (16). One possible reason for this difference is cell type: Huang et al. used HEK293 cells, whereas we used HeLa cells. Another reason may be related to use of exogenous trypsin; we often observed an unexpectedly high rate of infection in cells passaged using trypsin (data not shown). Therefore, we used a nonenzymatic cell dissociation solution rather than trypsin.

In the present study, we could not show the cleavage of SARS or NL63-S protein by TMPRSS2 because the cleavage products would be difficult to detect by Western blot analysis. We previously reported that a considerable amount of cleavage of SARS-CoV S protein was not detected, and Shulla et al. reported that only very low levels of S cleavage were detected in cells expressing TMPRSS2 (19, 27). Also, we previously reported that the S protein of mouse hepatitis virus type 2 (MHV-2), which is very similar to the S protein of SARS-CoV, is cleaved by trypsin only after conformational changes induced by receptor binding (21). Therefore, we hypothesized that only a small amount of S protein needs to be cleaved to enable viral or cell-cell membrane fusion by TMPRSS2.

Previous studies showed that SARS-CoV is able to enter cells

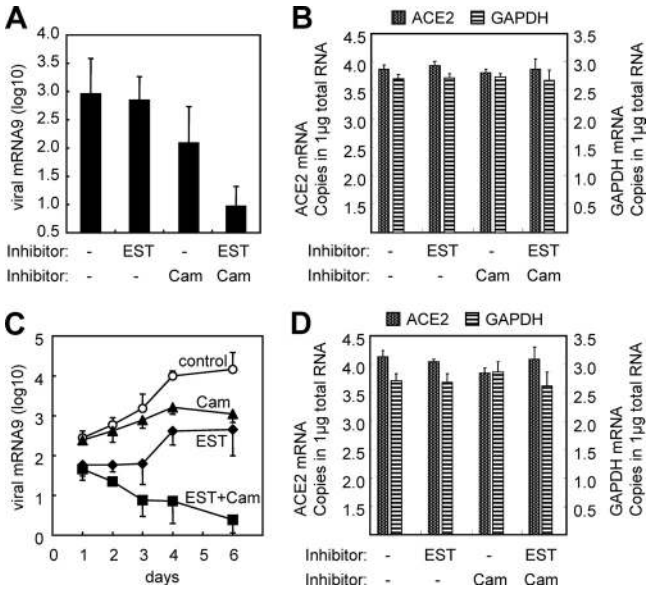

FIG 10 Inhibition of viral entry and multistep growth of SARS-CoV in Calu-3 cells after simultaneous treatment with inhibitors. (A) Calu-3 cells were infected with SARS-CoV at an MOI of 10 in the presence of 10 μM camostat (Cam), 10 μM EST, or both. Five hours later, cellular RNA was isolated and infectivity was quantified by real-time PCR. (B) The mRNA levels for a housekeeping gene (GAPDH) and for the virus receptor (ACE2) were measured to evaluate the nontoxicity of camostat and EST in the same Calu-3 cells for which the infectivity results are shown in panel A. (C) Calu-3 cells were infected with SARS-CoV at an MOI of 0.01 for 1 h at 37°C, and then the cells were incubated in the presence of 10 μM camostat, 10 μM EST, or both. Nontreated cells served as the negative control. Cellular RNA was isolated on the indicated days. (D) GAPDH and ACE2 mRNA levels were measured to evaluate the nontoxicity of camostat and EST in the samples at 6 days postinfection (shown in panel C). Infectivity was quantified by real-time PCR measurement of the amount of viral mRNA9. Error bars indicate the SD of the means from six independent samples.

via two distinct pathways, depending on the specific proteases present on the cell surface (19, 20, 30). As seen in Fig. 6, simultaneous treatment with EST and camostat significantly inhibited the entry of pseudotyped viruses into TMPRSS2-expressing HeLa cells, which suggests that both pathways must be blocked to prevent cell entry of SARS-CoV and HCoV-NL63. Also, the multistep growth of SARS-CoV in Calu-3 cells was significantly inhibited by simultaneous treatment with both inhibitors at 4 days and at 6 days, while separate treatment with camostat and EST caused only a partial decrease in SARS-CoV infection. This also indicates that both pathways need to be blocked to prevent SARS-CoV infection in lung-derived cells. On the other hand, we found that SARS-CoV enters Calu-3 cells through the cell surface (TMPRSS2) route rather than through the endosomal (cathepsins) route during initial viral entry, since siRNA targeting of TMPRSS2 caused a 5-fold decrease and camostat treatment caused a 10-fold decrease in SARS-CoV entry into Calu-3 cells, whereas viral entry was not blocked by EST (Fig. 9C and 10A). Therefore, it was unclear whether endosomal cathepsins or cell surface proteases are mainly utilized during viral entry.

Knowledge of which route (the cell surface, the endosome, or both) is mainly utilized by coronavirus in the human lungs will enable the choice of a suitable inhibitor, which could then be used as a candidate antiviral drug. It is important to note that SARS-CoV is highly pathogenic only in the lungs, although the receptor is expressed on the vesicular endothelial cells of all organs. This implies that lung-specific rather than ubiquitous enzymes determine viral tropism and pathogenesis. For example, SARS-CoV might utilize a lung-specific protease such as TMPRSS2 rather than cathepsins. This in turn suggests that camostat is a suitable candidate as an antiviral drug to prevent SARS-CoV infection in the lungs. Camostat is already being prescribed for the suppression of pancreatitis-induced pain due to its ability to inhibit pancreatic and other inflammatory proteases, including elastase (31). Therefore, camostat can inhibit *in vivo* infection by SARS-CoV and other pneumoviruses, such as influenza A and metapneumovirus virus, as all of these viruses are known to utilize TMPRSS2. Naturally, this strategy must first be confirmed in animal models.

ACKNOWLEDGMENTS

We thank Makoto Ujike (NVLU.ac.jp), Kazuhiko Kanou (NIH.go.jp), Masako Abe (NIH.go.jp), Koji Sakai (NIH.go.jp), and Makoto Takeda (NIH.go.jp) for valuable suggestions.

This work was financially supported by grants from the Ministry of Education, Culture, Sports, Science and Technology (Japan), the Ministry of Health, Labor and Welfare (Japan), the Mochida Memorial Foundation, and Telumo Life Science Foundation.

REFERENCES

1. **Belouzard S, Chu VC, Whittaker GR.** 2009. Activation of the SARS coronavirus spike protein via sequential proteolytic cleavage at two distinct sites. Proc. Natl. Acad. Sci. U. S. A. **106**:5871–5876.
2. **Belouzard S, Madu I, Whittaker GR.** 2010. Elastase-mediated activation of the severe acute respiratory syndrome coronavirus spike protein at discrete sites within the S2 domain. J. Biol. Chem. **285**:22758–22763.
3. **Bertram S, et al.** 2010. TMPRSS2 and TMPRSS4 facilitate trypsin-independent spread of influenza virus in Caco-2 cells. J. Virol. **84**:10016–10025.
4. **Bertram S, et al.** 2011. Cleavage and activation of the severe acute respiratory syndrome coronavirus spike protein by human airway trypsin-like protease. J. Virol. **85**:13363–13372.
5. **Bertram S, Glowacka I, Steffen I, Kühl A, Pöhlmann S.** 2010. Novel insights into proteolytic cleavage of influenza virus hemagglutinin. Rev. Med. Virol. **20**:298–310.
6. **Bosch BJ, Bartelink W, Rottier PJM.** 2008. Cathepsin L functionally cleaves the severe acute respiratory syndrome coronavirus class I fusion protein upstream of rather than adjacent to the fusion peptide. J. Virol. **82**:8887–8890.
7. **Böttcher E, Freuer C, Steinmetzer T, Klenk H-D, Garten W.** 2009. MDCK cells that express proteases TMPRSS2 and HAT provide a cell system to propagate influenza viruses in the absence of trypsin and to study cleavage of HA and its inhibition. Vaccine **27**:6324–6329.
8. **Böttcher E, et al.** 2006. Proteolytic activation of influenza viruses by serine proteases TMPRSS2 and HAT from human airway epithelium. J. Virol. **80**:9896–9898.
9. **Böttcher-Friebertshäuser E, et al.** 2010. Cleavage of influenza virus hemagglutinin by airway proteases TMPRSS2 and HAT differs in subcellular localization and susceptibility to protease inhibitors. J. Virol. **84**:5605–5614.
10. **Böttcher-Friebertshäuser E, Stein DA, Klenk H-D, Garten W.** 2011. Inhibition of influenza virus infection in human airway cell cultures by an antisense peptide-conjugated morpholino oligomer targeting the hemagglutinin-activating protease TMPRSS2. J. Virol. **85**:1554–1562.
11. **Chaipan C, et al.** 2009. Proteolytic activation of the 1918 influenza virus hemagglutinin. J. Virol. **83**:3200–3211.
12. **Choi S-Y, Bertram S, Glowacka I, Park YW, Pöhlmann S.** 2009. Type II transmembrane serine proteases in cancer and viral infections. Trends Mol. Med. **15**:303–312.
13. **Ding Y, et al.** 2003. The clinical pathology of severe acute respiratory syndrome (SARS): a report from China. J. Pathol. **200**:282–289.
14. **Fukushi S, et al.** 2005. Vesicular stomatitis virus pseudotyped with severe acute respiratory syndrome coronavirus spike protein. J. Gen. Virol. **86**:2269–2274.

15. **Glowacka I, et al.** 2011. Evidence that TMPRSS2 activates the severe acute respiratory syndrome coronavirus spike protein for membrane fusion and reduces viral control by the humoral immune response. J. Virol. **85**:4122–4134.
16. **Huang I-C, et al.** 2006. SARS coronavirus, but not human coronavirus NL63, utilizes cathepsin L to infect ACE2-expressing cells. J. Biol. Chem. **281**:3198–3203.
17. **Kam Y-W, et al.** 2009. Cleavage of the SARS coronavirus spike glycoprotein by airway proteases enhances virus entry into human bronchial epithelial cells in vitro. PLoS One **4**:e7870. doi:10.1371/journal.pone.0007870.
18. **Kawase M, Shirato K, Matsuyama S, Taguchi F.** 2009. Protease-mediated entry via the endosome of human coronavirus 229E. J. Virol. **83**:712–721.
19. **Matsuyama S, et al.** 2010. Efficient activation of the severe acute respiratory syndrome coronavirus spike protein by the transmembrane protease TMPRSS2. J. Virol. **84**:12658–12664.
20. **Matsuyama S, Ujike M, Morikawa S, Tashiro M, Taguchi F.** 2005. Protease-mediated enhancement of severe acute respiratory syndrome coronavirus infection. Proc. Natl. Acad. Sci. U. S. A. **102**:12543–12547.
21. **Matsuyama S, Taguchi F.** 2009. Two-step conformational changes in a coronavirus envelope glycoprotein mediated by receptor binding and proteolysis. J. Virol. **83**:11133–11141.
22. **Miyauchi K, Kim Y, Latinovic O, Morozov V, Melikyan GB.** 2009. HIV enters cells via endocytosis and dynamin-dependent fusion with endosomes. Cell **137**:433–444.
23. **Okumura Y, et al.** 2010. Novel type II transmembrane serine proteases, MSPL and TMPRSS13, proteolytically activate membrane fusion activity of the hemagglutinin of highly pathogenic avian influenza viruses and induce their multicycle replication. J. Virol. **84**:5089–5096.
24. **Paoloni-Giacobino A, Chen H, Peitsch MC, Rossier C, Antonarakis SE.** 1997. Cloning of the TMPRSS2 gene, which encodes a novel serine protease with transmembrane, LDLRA, and SRCR domains and maps to 21q22.3. Genomics **44**:309–320.
25. **Shirato K, Matsuyama S, Ujike M, Taguchi F.** 2011. Role of proteases in the release of porcine epidemic diarrhea virus from infected cells. J. Virol. **85**:7872–7880.
26. **Shirogane Y, et al.** 2008. Efficient multiplication of human metapneumovirus in Vero cells expressing the transmembrane serine protease TMPRSS2. J. Virol. **82**:8942–8946.
27. **Shulla A, et al.** 2011. A transmembrane serine protease is linked to the severe acute respiratory syndrome coronavirus receptor and activates virus entry. J. Virol. **85**:873–882.
28. **Simmons G, et al.** 2011. Different host cell proteases activate the SARS-coronavirus spike-protein for cell-cell and virus-cell fusion. Virology **413**:265–274.
29. **Simmons G, et al.** 2005. Inhibitors of cathepsin L prevent severe acute respiratory syndrome coronavirus entry. Proc. Natl. Acad. Sci. U. S. A. **102**:11876–11881.
30. **Simmons G, et al.** 2004. Characterization of severe acute respiratory syndrome-associated coronavirus (SARS-CoV) spike glycoprotein-mediated viral entry. Proc. Natl. Acad. Sci. U. S. A. **101**:4240–4245.
31. **Talukdar R, Tandon RK.** 2008. Pancreatic stellate cells: new target in the treatment of chronic pancreatitis. J. Gastroenterol. Hepatol. **23**:34–41.
32. **To KF, Lo AWI.** 2004. Exploring the pathogenesis of severe acute respiratory syndrome (SARS): the tissue distribution of the coronavirus (SARS-CoV) and its putative receptor, angiotensin-converting enzyme 2 (ACE2). J. Pathol. **203**:740–743.
33. **Watanabe R, et al.** 2008. Entry from the cell surface of severe acute respiratory syndrome coronavirus with cleaved S protein as revealed by pseudotype virus bearing cleaved S protein. J. Virol. **82**:11985–11991.
34. **Yoshikawa T, et al.** 2010. Dynamic innate immune responses of human bronchial epithelial cells to severe acute respiratory syndrome-associated coronavirus infection. PLoS One **5**:e8729. doi:10.1371/journal.pone.0008729.